Journal of Catalysis **184,** 499–513 (1999)
Article ID jcat.1999.2473, available online at http://www.idealibrary.com on IDEAL®

TAP Study of the Mechanism and Kinetics of the Adsorption and Combustion of Methane on Ni/Al_2O_3 and NiO/Al_2O_3

Olivier Dewaele[1] and Gilbert F. Froment[2]

Laboratorium voor Petrochemische Techniek, Universiteit Gent, Krijgslaan 281 S5, B9000 Gent, Belgium

Received November 19, 1998; revised March 5, 1999; accepted March 8, 1999

The activation of methane on an industrial Ni/Al_2O_3 catalyst was studied in a TAP reactor between 723 and 823 K. Methane adsorbs on the reduced Ni catalyst with an activation energy of 54 kJ mol^{-1}. Oxidation of the Ni on the surface of the support up to 13% results in a strong decrease of the methane adsorption rate which is more than proportional to the decrease in the number of reduced Ni sites on the surface. Three parallel pathways are responsible for the adsorption of methane on the oxidized Ni catalyst. Two pathways consist of hydrogen abstraction of methane by oxygen, reversibly chemisorbed on two different active sites. The lifetime of oxygen chemisorbed on the two active sites is limited due to desorption and amounts to respectively 5 and 148 s at 823 K. The rate of adsorption of methane via the third pathway decreases on a time scale of 1000 s. The type of site that is responsible for this pathway cannot be regenerated by oxygen. The combustion of methane on the oxidized catalyst was studied by means of step experiments with methane and isotopically labeled oxygen. Chemisorbed oxygen abstracts hydrogen from gas-phase methane and from adsorbed CH_x species. Lattice oxygen is responsible for the carbon-oxygen bond formation. The structure of the Ni/Al_2O_3 catalyst was studied by means of TPR, XPS, and XRD.

1. INTRODUCTION

Supported Ni catalysts are widely applied in the chemical industry, e.g., in steam reforming of natural gas to synthesis gas. The partial oxidation of natural gas on Ni catalysts is an interesting alternative route for synthesis gas production and the catalytic route is currently the subject of many studies (1–4). Although Ni catalysts have been extensively studied, many questions concerning the adsorption and activation of methane are not satisfactorily answered.

The adsorption of methane on reduced Ni has been thoroughly studied, also by means of surface science techniques using ideal single crystal surfaces and methane pressures up to 100 Pa. It was shown that methane adsorbs on the reduced Ni surfaces with an activation energy of about 53 kJ mol^{-1} (5–7). The reported dissociation probabilities vary from 10^{-12} to 10^{-3} at temperatures ranging from 300 to 400 K (5, 8). An important issue is the role of oxygen in the activation of methane on a reduced surface (6, 9). This was studied in an attempt to explain why the dissociation probabilities and adsorption rate coefficients of methane determined during studies of the partial oxidation or reforming of methane under industrial conditions are very high and of the same order as the sticking probability or adsorption rate coefficient of oxygen (5, 6, 8–11). The sticking probability of oxygen on reduced Ni is close to 1 (12–14). Currently, no agreement exists on the role of adsorbed oxygen in the activation of methane on reduced Ni (8, 9).

The mechanism of the adsorption and oxidation of methane on oxidized Ni catalysts has not been studied in great detail and a kinetic model is not available. This is surprising since it is well known that the catalyst at the inlet of the reactor is fully oxidized during the partial oxidation of methane over Ni catalysts (2, 3). In this region of the reactor, part of the methane feed is oxidized to CO_2 and H_2O. The remaining methane fraction is reformed by CO_2 and H_2O over the reduced catalyst, deeper in the reactor. The prediction of the steady state and transient behavior of an industrial catalytic partial oxidation reactor depends on the kinetic model for the methane activation on the oxidized catalysts. Also, the question remains whether or not the Ni catalyst needs to be completely reduced in order to partially oxidize or reform methane to synthesis gas.

Gavalas *et al.* (15, 16) studied the oxidation of methane over $NiO/\alpha Al_2O_3$ and NiO/ZrO_2. They observed a high methane combustion activity after oxidation of the reduced catalysts. The activity dropped to 30% of the original activity after 2 h. Gavalas *et al.* (15, 16) concluded from the analysis of the specific surfaces, from the changes in catalyst colors, and from their study of the structure of the catalysts that a decrease of the amount of excess O^{2-}, resulting from the oxidation of the catalysts, and the accompanying decrease in Ni^{3+} concentration are responsible for the lower activity. Recently, Hu and Ruckenstein (17) studied the

[1] Present address: UOP R&D, 25 East Algonquin Road, Des Plaines, IL 60017-5017.

[2] To whom correspondence should be addressed. Present address: Department of Chemical Engineering, Texas A&M University, College Station, TX 77843-3122. E-mail: Gilbert.Froment@skynet.be.

0021-9517/99 $30.00

TABLE 1

Overview of the Studied Subjects and of the Applied Techniques

Subject	Applied techniques
1. Structure of the catalyst	TPR
2. Gradual oxidation	Pulse titration
	TPR
3. Methane adsorption on the reduced catalyst	Single pulse experiments
	Modeling
4. Methane adsorption on the oxidized catalyst	Single pulse experiments
	Alternating pulse experiments
	Modeling
5. Oxygen adsorption on the oxidized catalyst	Single pulse experiments
	Pulse titration
	Modeling
6. Reaction of methane and oxygen on the oxidized catalyst	Step experiments
	Isotopically labeled oxygen

oxidation of methane over reduced and oxidized Ni catalysts by means of broadened-pulse response and isotopic experiments. They concluded that methane and oxygen react on the oxidized catalyst via an Eley-Rideal mechanism in which the gas phase or weakly adsorbed methane reacts with adsorbed oxygen. The results of Gavalas *et al.* (15, 16) and Hu and Ruckenstein (17) were determined on different time scales. Gavalas *et al.* (15, 16) found a response time of several hours. Hu and Ruckenstein (17) showed that at 1073 K the lifetime of the adsorbed oxygen was of the order of minutes.

Within the framework of developing simulation models for the catalytic partial oxidation of methane, the present study deals with the adsorption of methane on a reduced Ni catalyst and the combustion of methane on the oxidized Ni catalyst. After the determination of the structure of the Ni catalyst following different pretreatments, the adsorption of methane on the reduced catalyst and the influence of gradual oxidation on the methane adsorption rate were studied. Thereafter, experiments were performed to study the adsorption of methane on the oxidized catalyst. During these experiments, a strong influence of feeding gas-phase oxygen on the methane adsorption rate under vacuum was observed. Finally, the reaction of both methane and oxygen on the oxidized catalyst was studied. Table 1 gives an overview of the applied techniques.

2. METHODS

The activation of methane on the oxidized and reduced Ni/Al_2O_3 catalyst was studied by means of temporal analysis of products (TAP). The TAP reactor system, constructed by Autoclave Engineers Inc., consists of a sequence of three vacuum chambers. The first chamber contains a small reactor, 40 mm long and 5 mm in diameter. The entrance of this reactor is connected via a small inlet volume with two pulse valves and two continuous feed valves. The pulse valves allow the rapid injection of very small amounts of reactant. The pulse size can be varied between 10^{13} and 10^{17} molecules. The injection time is less than 100 μs. The background pressure in the reactor chamber is about 10^{-4} to 10^{-5} Pa and is mainly caused by the presence of N_2 and H_2O. The second chamber is the differential chamber. Molecules that do not travel in a straight line from the exit of the reactor to the third chamber or analysis chamber are trapped here and pumped away. This differential chamber also acts as a prevacuum chamber for the analysis chamber. The pressure in the differential chamber is about 10^{-6} Pa. The responses of the reactant and of the products at the exit of the reactor are measured with a UTI 100C quadrupole mass spectrometer located in the analysis chamber. The time resolution at which the evolution of the flux at the outlet of the reactor can be measured is less than 1 ms. The pressure in the analysis chamber is 10^{-7} Pa. This ensures that the signal detected with the mass spectrometer is proportional to the flux at the outlet of the reactor. A more detailed description of the TAP reactor can be found elsewhere (18).

Several types of experiments were performed in the TAP equipment. The structure of the Ni catalyst was mainly studied by means of *temperature programmed reduction* (TPR). For this purpose the reactor was operated under vacuum, heated at a rate of 10 K min^{-1}, and fed by 4×10^{-7} mol s^{-1} hydrogen. The signal at AMU 18, representative for water, was continuously monitored during heating. The adsorption of methane on the reduced catalyst and of oxygen on the oxidized catalyst was studied by means of *single pulse experiments*. During these experiments, a train of 10 to 20 small CH_4/Ar pulses was injected into the reactor at a frequency of 1 to 2 pulses per second. Each pulse contained 10^{14} to 10^{15} molecules, which is more than a factor 10^3 to 10^4 lower than the number of active sites in the reactor. This low pulse size ensures that transport occurs by Knudsen diffusion and that the catalyst state does not change due to reaction with methane or saturation by oxygen. Each pulse response in the response train is identical since the catalyst state does not change. The noise to signal ratio was decreased by using the average response. The adsorption and combustion of methane on the oxidized catalyst were studied by means of *single pulse experiments*, *alternating pulse experiments*, and *step experiments*. In an alternating pulse experiment, two pulse trains of the same frequency but of two different reactants are simultaneously injected in the reactor. The time between the injection with one pulse valve and with the other pulse valve can be varied. This experiment is performed to study the interaction of one reactant with intermediates created on the surface by the other reactant. The lifetime of the intermediates on the surface can be studied by varying the time between the injections of both pulse valves. A step experiment was performed by

TABLE 2

Composition of the Ni/Al_2O_3 Catalyst as Received

Component	wt%
Ni	19 ± 2
Al_2O_3	50–55
TiO_2	13–15
CaO	5.5–7.5
SiO_2	<0.20
C	<0.10
S	<0.05
Cl	<0.02
Fe_2O_3	<0.10
Other alkali metals	<0.05
Other heavy metals	<0.10

continuously injecting reactant from one pulse valve. The pulse period was much smaller than the residence time in the reactor. Using the pulse valve instead of the continuous feed valves allows operation at low and stable feed rates.

The catalyst is an industrial Ni/Al_2O_3 catalyst in the form of Rashig rings, similar to the one used by Dissanayake *et al.* (2). The rings were crushed and the particles were sieved. The fraction with particle sizes between 0.25 and 0.50 mm was retained for the experiments. The catalyst bed was diluted with quartz particles with a diameter between 0.25 and 0.50 mm and the catalyst/quartz mixture was packed between quartz packings at the inlet and at the outlet of the reactor. The BET surface of the catalyst is between 10 and 30 $m_c^2\,g^{-1}$. SEM results show that the pore size is about 1 to 2 μm. This excludes diffusion limitations inside the particles. The bulk density of the catalyst is 880 $kg\,m_c^{-3}$. The composition of the catalyst is summarized in Table 2. Prior to all experiments, the catalyst was reduced with a TPR experiment extending to 1138 K. The catalyst was kept at 1138 K in the hydrogen flow until the water flux at the exit of the reactor was hardly detectable.

3. RESULTS AND DISCUSSION

3.1. Structure of the Ni Catalyst

The amount of surface Ni atoms on the catalyst was determined with the TAP reactor by means of chemisorption of oxygen on the reduced Ni catalyst at different temperatures. The results of Müller (19) and Hoang-Van *et al.* (20) show that the determination of the dispersion of Ni catalysts can be done by means of oxygen chemisorption at room temperature assuming an O/Ni_S, ratio equal to 2. The amount of oxygen adsorbed at room temperature on 0.060 g of reduced catalyst is 2.63×10^{-6} mol. Taking the composition of the Ni catalyst into account this leads to a dispersion of 1.4%, a very low value. The results of Zielinski (21) and Huang *et al.* (22) show that not all the metallic Ni is located on the surface of the support after reduction at high temperatures. A large fraction of the metallic Ni is incorporated in or covered by the Al_2O_3 support (21, 22). Therefore, it can be expected that the dispersion of the Ni on the surface of the support is much higher than the dispersion of the total amount of Ni in the catalyst. To determine the total amount of Ni on the support the catalyst was reduced at 1138 K and oxidized by means of an oxygen pulse train at 823 K. The total amount of oxygen taken up by 0.060 g of catalyst during the oxidation is 2.05×10^{-5} mol. Since the ratio O/Ni is 1 after oxidation, the total amount of Ni on the support is 4.10×10^{-5} mol. This is much lower than the amount of Ni in the catalyst, which is about 1.92×10^{-4} mol. Only 21% of the Ni in the catalyst is located on the surface of the support. The other Ni fraction is incorporated in the Al_2O_3 support. The dispersion of the Ni on the surface of the support is 6.7%. This corresponds to a crystal size of about 13.4 nm.

The second technique used to study the structure of the Ni catalyst is TPR. The results of De Bokx *et al.* (23) show that this technique is very valuable for determining the state of the Ni on the oxidized catalyst. TPR of the catalyst as received yielded a spectrum with a peak at 903 K and a peak at 1103 K. These peaks correspond to the reduction of $NiAl_2O_4$ spinel with different degrees of crystallinity (24). To obtain a better insight into the structure of the catalyst after reduction at high temperatures, the reduced catalyst was oxidized by injection of a pulse train of oxygen at 823 K until the oxygen conversion dropped to zero or by a feed of oxygen for 3 h at 823 K. Bulk spinel is not formed at 823 K (15, 21, 24). TPR after oxidation at 823 K results in a spectrum with a peak at 683 K and a shoulder at 823 K (Fig. 1). De Bokx *et al.* (23) reported TPR spectra of NiO/Al_2O_3 catalysts with peaks at 673 and 793 K. This is in agreement with the results reported here. De Bokx *et al.* (23) identified the

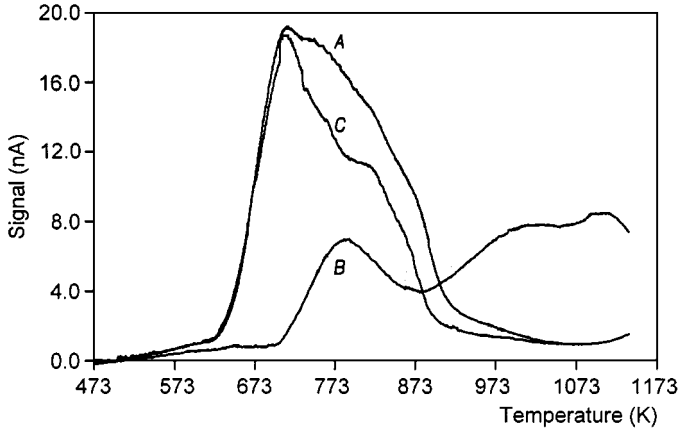

FIG. 1. TPR spectra of 0.060 g Ni catalyst oxidized at 823 K (A), oxidized at 823 K followed by heating to 1123 K for 30 min (B), and oxidized at 823 K, heated to 1123 K, reduced to 1138 K (TPR), and oxidized at 823 K (C).

peak at 673 K as reduction of large NiO crystallites on the Al_2O_3 surface. The peak at 793 K was associated with the reduction of $NiAl_2O_4$ surface spinel (23). The same TPR experiment was repeated to verify if a slow transformation of the NiO catalyst occurred as a function of time after oxidation. The reduced catalyst was oxidized with 600 pulses of oxygen. The time between the oxidation and the TPR was varied. The TPR spectra did not change with time after oxidation at 823 K. This proves that no bulk $NiAl_2O_4$ is produced after oxidation at 823 K. Literature data show that this conversion occurs only at temperatures above 873 K (15, 21, 24). Heating of the oxidized catalyst above 1073 K or oxidizing the catalyst above 1073 K resulted in TPR spectra which are strongly shifted to higher temperatures (Fig. 1, curve B). The longer the catalyst was held at 1073 K, the higher the peak temperatures in the spectra, indicating a higher crystallinity of the $NiAl_2O_4$ (15, 16, 21).

The most interesting result was generated by an experiment in which the Ni catalyst was oxidized at 823 K by a continuous feed of oxygen and in which this oxidized sample was heated to 1123 K for 30 min. Prior to this experiment, a TPR spectrum of the catalyst oxidized at 823 K was determined. After heating to 1123 K, the TPR spectrum of this sample was determined and the catalyst was oxidized again at 823 K. The TPR spectrum of this oxidized sample was also determined. Figure 1 shows the TPR spectra. From this figure, it is clear that heating up to high temperatures, followed by reduction at high temperatures and oxidation at 823 K, results in an oxidized Ni catalyst containing less surface spinel. The amount of bulk NiO on the surface remains the same. XRD and XPS experiments were performed to understand what happens with the Ni fraction corresponding with the shoulder in the TPR spectrum. Two Ni samples, oxidized at 823 K, were prepared. The first sample was not treated at high temperatures after oxidation. The second sample was oxidized at 823 K, heated to 1123 K, reduced by means of TPR extending to 1138 K, and oxidized again at 823 K. XPS experiments could not reveal any significant differences between both samples. The XRD experiments showed that both samples contained reduced Ni, even after oxidation at 823 K. The sample which was not heated after oxidation, contained less reduced Ni than the sample that was heated after oxidation. This shows that heating the oxidized catalyst to 1123 K, followed by reduction by means of TPR extending to 1138 K, results in the incorporation into the support of the Ni fraction that is oxidized at 823 K into surface spinel. This Ni fraction cannot be oxidized at 823 K after reduction at high temperatures. These results point toward an increase of the thickness of the Al_xO_y layer, which is covering the Ni after reduction of the $NiAl_2O_4$ surface spinel, decreasing the accessibility of oxygen to the reduced Ni.

Although the decrease in the amount of Ni on the support results in a decrease in oxygen sorption capacity at room temperature, no influence on the methane activation rate was observed. This is an additional indication that the Ni fraction responsible for the shoulder in the TPR spectrum is indeed surface $NiAl_2O_4$ spinel which is not active for methane activation after oxidation and which is partially covered by a layer of Al_xO_y after reduction, also resulting in a low methane activation rate. Based on the results presented here and on literature data (21, 23, 25), the structure of the Ni catalyst shown in Fig. 2 is proposed.

3.2. Gradual Reoxidation of the Ni Catalyst

An important parameter in the study of the methane activation on the Ni catalyst is the degree of oxidation of the Ni on the alumina support. The sticking probability of oxygen on Ni is very high (12–14). Gradual oxidation of the Ni on the support by injection of a limited amount of oxygen at 823 K is not useful. This would result in a reactor with NiO at the entrance and reduced Ni at the exit. A uniform degree of oxidation throughout the reactor can be obtained by repeatedly saturating the Ni catalyst with oxygen at room temperature followed by heating the catalyst to 823 K under vacuum for 15 min. The results of Müller (19) show that heating does not result in desorption of oxygen, but in incorporation of oxygen in the bulk of the Ni. Indeed, oxygen desorption was not observed during the heating of the Ni samples. As mentioned previously, the O/Ni_s ratio at room temperature is 2. The dispersion of Ni on the surface of the support is about 6.7%, leading to a degree of oxidation after the first saturation and heating of 13.4%. The relative decrease of the sorption capacity corresponds well with the increase of the degree of oxidation. This shows that oxygen only adsorbs on the reduced Ni sites and that the oxygen is distributed uniformly through the bulk of the Ni on the surface of the alumina support at 823 K. TPR of the Ni catalyst as a function of the degree of oxidation reveals a strong increase of the TPR peak temperature with higher degrees of oxidation ranging from 623 K at 13% oxidation to 683 K at 100% oxidation (Fig. 3). This can be explained by the reduction of NiO by hydrogen activated on reduced Ni. At low degrees of oxidation only a very small shoulder in the TPR spectrum can be observed. A possible explanation would be that at 823 K it is difficult to oxidize the Ni fraction that is reduced at that temperature. It seems more likely that the surface spinel is only produced from a given degree of oxidation onward.

3.3. Methane Adsorption on the Reduced Catalyst

The adsorption of methane on the reduced Ni catalyst was studied under vacuum by means of single pulse experiments with a CH_4/Ar mixture. The methane pulse size was very small, resulting in irreversible methane adsorption and transport by Knudsen diffusion. The ratio of the pulse size

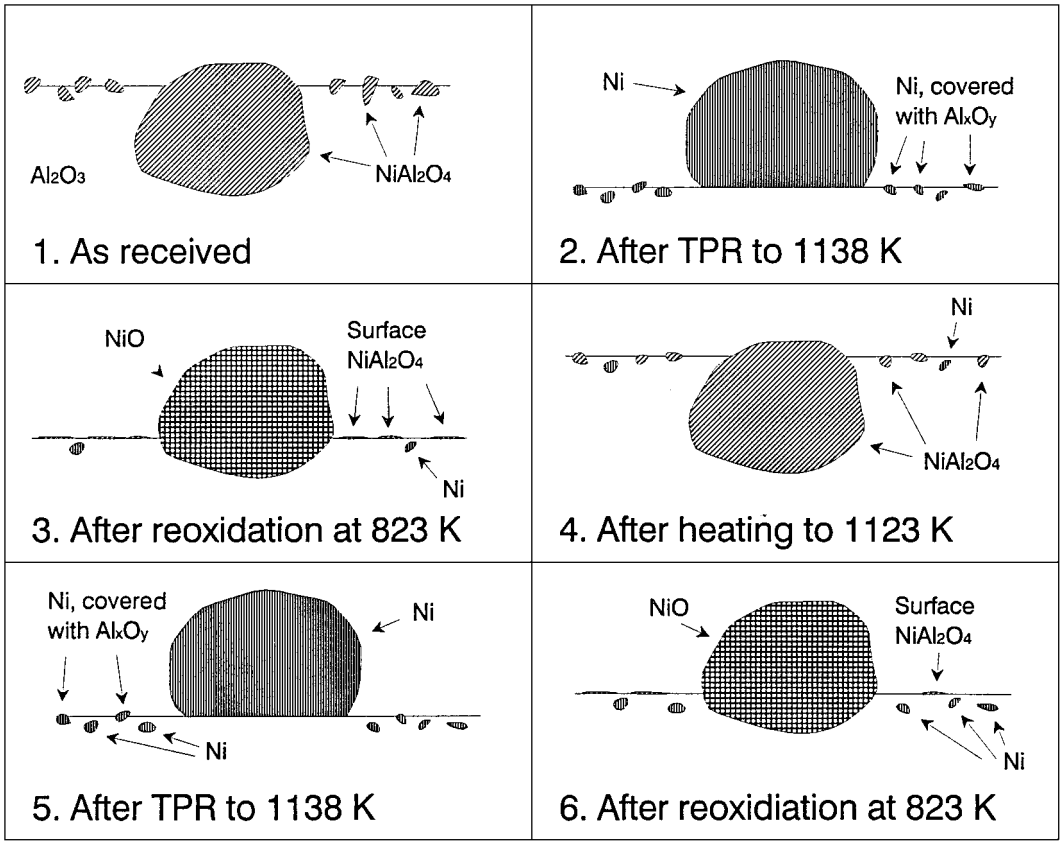

FIG. 2. Interpretation of the structure of the Ni catalyst as a function of the pretreatment.

to the amount of active sites in the reactor is about 10^{-3} to 10^{-4}, too low to allow second-order elementary steps, such as desorption of hydrogen, to proceed rapidly. This is why no reaction products were observed during the experiments over the reduced catalyst. Moreover, the formation of filamentous carbon cannot be excluded during pulse experiments with high methane pulse sizes (26). With the small pulse size the methane activation is irreversible. Hydrogenation of carbon, which is also a higher order reaction, is too slow due to the low surface coverage. The methane pulse conversion was determined from the zeroth order moments of the methane and argon pulse responses.

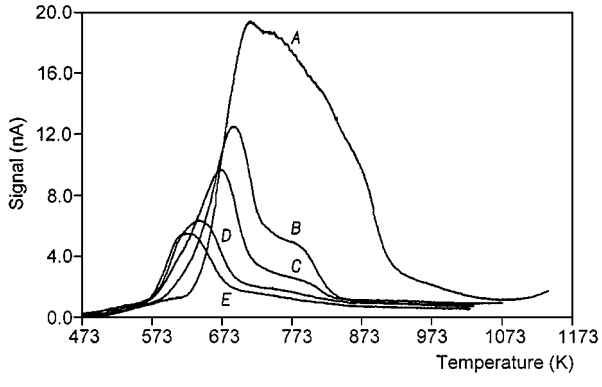

FIG. 3. TPR spectra of the Ni catalyst surface oxidized by adsorbing oxygen at room temperature followed by heating to 823 K for 15 min. (A) Completely surface oxidized at 823 K; (B) 12 adsorption and heating cycles; (C) 6 cycles; (D) 2 cycles; (E) 1 cycle.

The conversion of the methane pulse at 823 K over 0.060 g of Ni catalyst depends on the reduction procedure. TPR up to 873 K of a Ni sample oxidized at 823 K, followed by a continuous feed of hydrogen for 1 h at 873 K, results in 87% conversion. Heating the sample under vacuum at 823 K for 2 h decreases the methane conversion to 80%. Injecting hydrogen restores the initial methane adsorption rate. Presumably, the catalyst is not completely reduced after TPR up to 873 K. Diffusion of oxygen from the Ni bulk to the Ni surface during heating at 823 K decreases the number of methane adsorption sites. The conversion of the methane pulses at 823 K after TPR up to 973 K amounts to 93%. After TPR up to 1138 K, a conversion of 88% was observed. The decrease in conversion associated with higher reduction temperatures can be explained in terms of the coverage of part of the Ni by TiO_x or by Al_xO_y, as discussed in Section 3.1. Most likely, this Ni fraction consists of small Ni crystallites on the surface. Table 3 is an overview of the observed methane pulse conversion after various reduction pretreatments.

TABLE 3

Conversion of the Methane Pulses Observed during Single Pulse Experiments on 0.060 g Reduced Ni Catalyst as a Function of the Highest Temperature during Reduction by Means of TPR

Highest temperature during TPR	Methane conversion at 823 K
873 K	84%
1023 K	93%
1138 K	86%

The methane conversion over 0.060 g of Ni catalyst reduced at 1138 K increases with temperature from 69% at 723 K to 88% at 823 K. The methane adsorption rate coefficient k_a ($m_r^3\ kg_c^{-1}\ s^{-1}$) was calculated from the conversion, x, by means of the following equation:

$$x = 1 - \frac{1}{L_c\sqrt{\frac{\varepsilon_c \rho_B k_a}{D_c}}\sinh\left(L_c\sqrt{\frac{\varepsilon_c \rho_B k_a}{D_c}}\right)\frac{L_e D_c}{L_c D_e} + \cosh\left(L_c\sqrt{\frac{\varepsilon_c \rho_B k_a}{D_c}}\right)}. \quad [1]$$

Equation [1] is derived from the analytical calculation of the zeroth order moment of the methane pulse responses by means of Laplace transform of the continuity equation for gas phase methane. L_c and L_e (m_r) are the lengths of the catalyst packing and of the quartz bed at the exit, ε_c ($m_g^3\ m_r^{-3}$) is the void fraction of the catalyst bed, D_c and D_e ($m_g^3\ m_r^{-3}\ s^{-1}$) are the Knudsen diffusivity in the catalyst bed and in the quartz bed at the exit, and ρ_B ($kg_c\ m_r^{-3}$) is the bulk density of the catalyst bed in the reactor. The factor $L_e D_c L_c^{-1} D_e^{-1}$ was about 1 for the experiments discussed here.

The Arrhenius plot for the adsorption rate coefficient of methane on the Ni catalyst after TPR up to 1138 K is shown in Fig. 4. The activation energy for methane adsorption is found to be 54 ± 4 kJ mol^{-1}. The adsorption rate coefficient at 773 K is 1.28 $m_r^3\ kg_c^{-1}\ s^{-1}$. Beebe *et al.* (5) and Alstrup *et al.* (6) found an activation energy of respectively 54 and 52 kJ mol^{-1}.

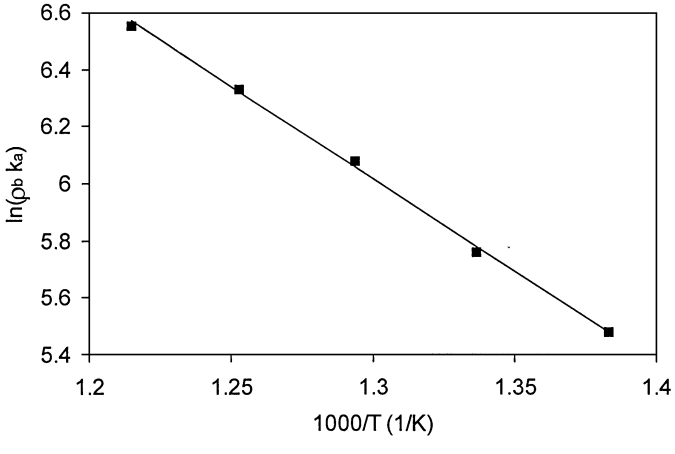

FIG. 4. Arrhenius plot of the methane adsorption rate coefficient $\rho_B\ k_a$ (s^{-1}) on the reduced Ni catalyst.

The degree of oxidation has a very strong influence on the methane adsorption rate. The methane conversion at 823 K over 0.060 g of Ni catalyst, reduced at 1138 K, drops from 88 to 7% after oxidizing the Ni on the surface of the support to a degree of oxidation of about 13%. Increasing the degree of oxidation to 20% results in an almost complete deactivation of the catalyst. The adsorption rate coefficient of methane at 773 K on the catalyst after 13% oxidation is 0.018 $m_r^3\ kg_c^{-1}\ s^{-1}$. The activation energy for methane adsorption is estimated to be 24 ± 20 kJ mol^{-1}. The decrease of the adsorption rate coefficient by a factor of more than 50 is more than proportional to the small decrease of the number of available sorption sites. These results are in agreement with results obtained during the study of the partial oxidation of methane over a Rh/Al_2O_3 catalyst, from which it was suggested that the activation of methane on Rh is a structure-sensitive reaction (27). Only a limited number of sites, presumably defects on the Rh surface, would be active for methane activation (27). They are preferentially deactivated by carbon or by deposition of TiO_x (27). This is proposed to be valid for the Ni catalyst also. The limited number of Ni sites which are very active for methane dissociation are preferentially deactivated by oxygen adsorption. Additional support of this structure sensitivity can be found in studies of methane activation on single crystal surfaces from which it was shown that the methane sticking probability very strongly depends on the nature of the Ni surface (5, 8, 28). The pronounced decrease of the methane activation rate on the partially reduced Ni at low degrees of reoxidation supports the model proposed by De Groote and Froment (29) for the partial oxidation of methane over a Ni catalyst. In their model, the rates of the reforming reactions and the water-gas shift reaction account for the degree of oxidation of the catalyst through the introduction of a multiplication factor x_{O2}^{12}, with x_{O2} the fractional oxygen conversion.

3.4. Methane Adsorption on the Surface-Oxidized Catalyst

3.4.1. Qualitative Aspects

The adsorption of methane on the oxidized catalyst was studied after oxidation of the reduced Ni catalyst at 823 K. The catalyst was oxidized by an oxygen flow of 5×10^{-7} mol s^{-1} or by injection of a large number of oxygen pulses until no further oxygen uptake could be observed. The results presented in Section 3.1 show that this oxidation procedure leads to a surface-oxidized catalyst in which the Ni on the surface of the support is completely oxidized and the Ni fraction that is located in the bulk of the support remains reduced. The methane adsorption activity was determined

in the presence and absence of gas-phase oxygen. Data of Hutchings and Scurrell (30) confirm that methane is mainly activated by NiO and not by CaO, Al_2O_3, or TiO_2, which are also present in the catalyst.

The methane adsorption rate at 823 K was measured by means of single pulse experiments with a CH_4/Ar mixture. The pulse size was of the order of 10^{14} molecules. Only then the reaction does not modify the catalyst state. This was confirmed by repeating the experiment with a different pulse size or with a different number of pulses in the pulse train. The results were always the same. Immediately after oxidation of 0.060 g Ni catalyst at 823 K, a conversion of the methane pulse of 13% was observed. Holding the catalyst under vacuum at 823 K for several hours resulted in a decrease of the methane conversion to 0%. In another experiment, methane was injected in a flow of 10^{-6} mol s^{-1} of oxygen immediately after oxidation at 823 K. In this case, the methane conversion amounted to 30%. The first vacuum experiments after oxidation were performed about 10 to 20 s after oxidation. This means that the decrease of the conversion from 30 to 13% occurs on a time scale of maximum 10 s, which is much smaller than the time scale at which the conversion decreases from 13 to 0%.

The methane adsorption activity after reoxidation and its decrease on a time scale of less than 10 s followed by a slower decrease on a time scale of 100 to 1000 s show that one or more types of sites or different pathways for methane adsorption exist on the catalyst after oxidation of the Ni on the surface of the support. When oxygen was continuously fed to the reactor the adsorption rate was equal to the adsorption rate under vacuum immediately after feeding oxygen, indicating that all these sites or pathways are also active for methane adsorption in the presence of gas phase oxygen.

(a) Activity decay on a time scale of 100 to 1000 s. The activity decay on a time scale of 100 to 1000 s was studied by means of single pulse experiments with methane after surface oxidation of 0.060 g of Ni catalyst at 823 K. The conversion of the methane pulses was measured as a function of time following oxidation. It is important to note that the methane pulses were small, resulting in an insignificant change of the catalyst state due to reaction with methane.

The observed evolution of the methane conversion after oxidation is shown in Fig. 5. Two zones can be distinguished: one zone in which the activity decays on a time scale of 100 s and a second zone in which the activity decays on a time scale of 1000 s. Although the pulse size was very low compared to the amount of Ni atoms on the reduced surface, it is still possible that the amount of active sites on the oxidized catalyst is low compared to the methane pulse size. If this is true, the change in activity as a function of time following oxidation can still be caused by conversion of methane. The same experiment with a different number of single pulse experiments or with a different pulse size

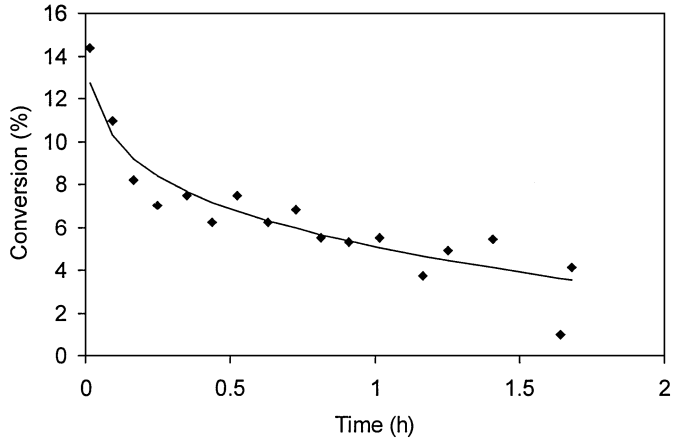

FIG. 5. Evolution of the methane conversion at 823 K on 0.060 g of surface-oxidized catalyst in the absence of gas-phase oxygen as a function of time after surface oxidation. The methane pulse size: 2.04×10^{14} molecules. (◆) Experimental; (—) modeled according to Section 3.4.2.b.

was repeated. The same evolution of the conversion was observed, showing that the variation in conversion is not caused by reaction with methane.

A similar experiment but with intermediate feeding of gas phase oxygen was also performed. The catalyst was oxidized at 823 K and the methane conversion was monitored as a function of time following oxidation. After a certain time, oxygen was fed to the reactor for 5 to 20 min. Thereafter, the conversion of methane in the absence of gas-phase oxygen was continuously measured, again as a function of time. This was repeated several times during one experiment. Figure 6 shows the evolution of the methane conversion as a function of time after oxidation in the absence of gas-phase oxygen and shows the impact of feeding gas-phase oxygen. The oxygen fed regenerates the

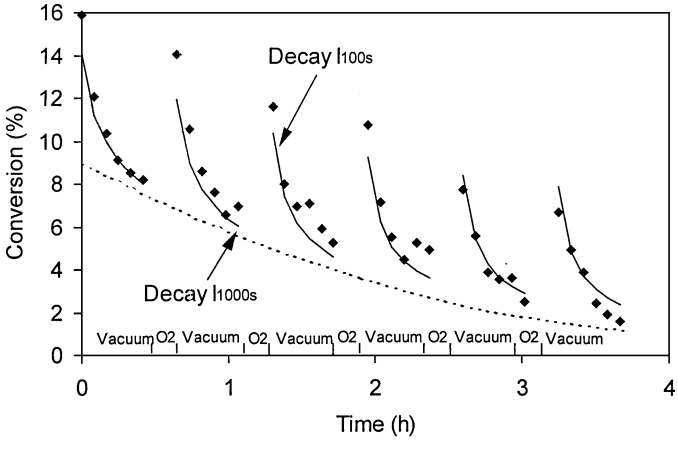

FIG. 6. Evolution of the methane conversion at 823 K on 0.060 g of surface-oxidized catalyst as a function of time after surface oxidation. Oxygen was fed (10^{-6} mol s^{-1}) for 10 min every 35 min. (◆) Experimental; (—) modeled according to Section 3.4.2.b.

activity which decays as a function of time on a time scale of 100 s. The decay on a time scale of 1000 s, shown in Fig. 6 as the dotted line, is not influenced by the gas-phase oxygen feed.

These results show that methane is activated under vacuum via two pathways after oxidation of the catalyst. These pathways can correspond to two different active sites for methane activation or to two different reactive intermediates adsorbed on one type of site. Another explanation for the existence of the two different time scales according to which the methane adsorption activity decreases is the existence of two different mechanisms at which a single type of active species for methane adsorption on the surface is being depleted. However, if the latter were true, then the original total methane adsorption activity should be restored after feeding oxygen to the reactor. The observation that the activity which decays on a time scale of 100 s can be regenerated independently of the activity of the pathway which decays on a time scale of 1000 s is evidence that the two pathways are caused by two different and independent sites. These sites will be denoted as $l_{100\,s}$ and $l_{1000\,s}$. The index refers to the lifetime of their activities under vacuum. Repeating the same experiment with feeding oxygen more or less frequently or for a longer or shorter time confirms that the activity decays of both pathways are independent of one another. The fact that the sites $l_{100\,s}$ can be regenerated by an oxygen feed strongly indicates that methane is activated on these sites through interaction with reversibly chemisorbed oxygen. This chemisorbed oxygen is probably O^- or O^{2-} (31–33). The decay of the activity for methane adsorption of $l_{100\,s}$ under vacuum is then caused by desorption of oxygen. The amount of sites $l_{100\,s}$ remains constant. The irreversible decay of the activity of $l_{1000\,s}$ indicates that the number of these sites decreases with time.

(b) Activity decay on a time scale of 10 s. A third pathway for methane adsorption with an activity decrease on a time scale of 10 s exists in the presence of gas-phase oxygen. This pathway was further studied by simultaneous injection of methane and oxygen over 0.20 g of Ni catalyst which was surface-oxidized at 823 K and kept under vacuum for several hours. The pulse size of methane was of the order of 10^{14} molecules. The pulse size of oxygen was varied between 0 and 3×10^{16} molecules. The results show that an oxygen pulse size larger than 1.5×10^{16} molecules is sufficient to take the activity of the catalyst to its maximum value, identical to that reached in the presence of a continuous flow of oxygen. Based on this result, an alternating pulse experiment was performed in which methane and oxygen were injected separately over 0.20 g surface oxidized catalyst at 823 K and in which the time between the oxygen and the methane pulse was varied. The oxygen and methane pulse sizes composed respectively 5×10^{16} and 10^{14} molecules. The oxidized catalyst was kept under vacuum for 2 h at 823 K prior to the experiment. The decrease in the adsorption rate coefficient was calculated using Eq. [1] and was corrected for the decrease due to the decay in activity of the sites $l_{100\,s}$ and $l_{1000\,s}$. The latter was done using the model for the activity for $l_{100\,s}$ and $l_{1000\,s}$ described in Section 3.4.2.b. Figure 7 shows the corrected decay in activity for methane adsorption. The time constant for this decay is of the order of 10 s.

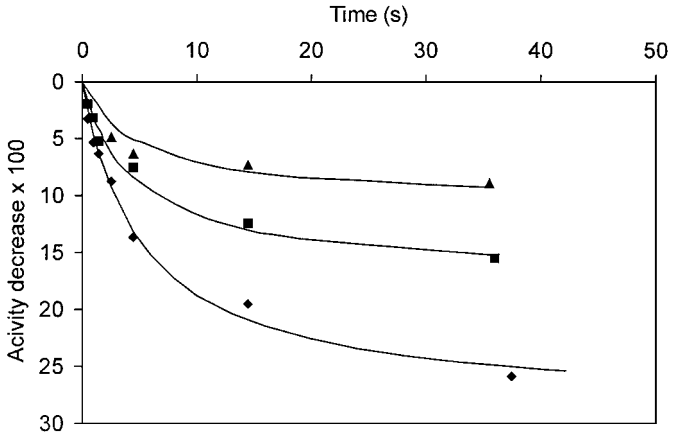

FIG. 7. Decrease of the methane absorption activity of the sites $l_{10\,s}$ at 823 K (◆), 773 K (■), and 723 K (▲) observed on 0.20 g of surface-oxidized catalyst, expressed as $\varepsilon_c \rho_B\ k_a\ L_c^2 D_c^{-1}$, as a function of the time interval between the oxygen and the methane pulse. (—) Modeled according to Section 3.4.2.c.

The results presented above show that a second type of adsorbed oxygen species which interact with gas-phase methane is adsorbed on the surface. Again, it can be assumed that this chemisorbed oxygen is O^- or O^{2-} (31–33). The lifetime of this adsorbed oxygen is of the order of 10 s at 823 K. This second oxygen species can occupy $l_{100\,s}$ sites or a third type of site. Studying the adsorption of oxygen on the oxidized catalyst will show that the latter is true (Section 3.5). The active sites that are responsible for this third methane adsorption pathway will be represented by $l_{10\,s}$.

3.4.2. Modeling

(a) Model equations. The adsorption rate of methane $r_{a,i}$ (mol $kg_c^{-1}\,s^{-1}$) on the different sites $l_{10\,s}$, $l_{100\,s}$, and $l_{1000\,s}$ can be expressed as

$$r_{a,i} = \varepsilon_c k_{a,i} \theta_i C_{CH_4}. \qquad [2]$$

The subscript i stands for sites with either 10, 100, or 1000 s lifetime, $k_{a,i}$ ($m_r^3\,kg_c^{-1}\,s^{-1}$) the adsorption rate coefficient on site l_i, θ_i the coverage of site l_i with oxygen or the fraction of the sites l_i still active for methane dissociation, and C_{CH_4} the gas-phase concentration methane (mol m_g^{-3}).

The total adsorption rate of methane r_a (mol $kg_c^{-1}\,s^{-1}$) and the corresponding adsorption rate coefficient

k_a ($m_r^3\ kg_c^{-1}\ s^{-1}$) can be represented as in Eqs. [3] and [4]:

$$r_a = \varepsilon_c k_a C_{CH_4}$$
$$= \varepsilon_c (k_{a,10\,s}\theta_{10\,s} + k_{a,100\,s}\theta_{100\,s} + k_{a,1000\,s}\theta_{1000\,s}) C_{CH_4} \quad [3]$$
$$k_a = k_{a,10\,s}\theta_{10\,s} + k_{a,100\,s}\theta_{100\,s} + k_{a,1000\,s}\theta_{1000\,s}. \quad [4]$$

The rate of decay, $r_{d,10\,s}$ and $r_{d,100\,s}$ (mol $kg_c^{-1}\ s^{-1}$), by desorption of oxygen from the sites $l_{10\,s}$ and $l_{100\,s}$, or the rate of decay of $l_{1000\,s}$, $r_{d,1000\,s}$ (mol $kg_c^{-1}\ s^{-1}$), is written

$$r_{d,i} = k_{d,i}\theta_i^{n_i} C_{t,i}, \quad [5]$$

with $k_{d,i}$ (s^{-1}) the oxygen desorption or decay rate coefficient for the site l_i, n_i the order of $r_{d,i}$ in θ_i and $C_{t,i}$ (mol kg_c^{-1}) the concentration sites l_i.

During the experiments in the absence of gas-phase oxygen, small methane pulse sizes were applied, so that the decay in activity is only caused by desorption of oxygen or by deactivation. This results in the following differential equation

$$\frac{d\theta_i}{dt} = -k_{d,i}\theta_i^{n_i}, \quad [6]$$

in which θ_i represents the fractional coverage by oxygen of either the sites $l_{10\,s}$ and $l_{100\,s}$ or the fraction of sites $l_{1000\,s}$ which are still active.

Values of 1 and 2 for the order n_i of $r_{d,i}$ in θ_i were considered corresponding to first- or second-order deactivation or desorption of the adsorbed oxygen species. Integration of Eq. [6] with θ_i equal to 1 as the intial condition results in the Eqs. [7] and [8] for θ_i as a function of time following oxidation in the case of $l_{1000\,s}$ and after feeding oxygen in the case of $l_{10\,s}$ and $l_{100\,s}$.

$$\theta_i = e^{-k_{d,i}t} \quad n_i = 1 \quad [7]$$

$$\theta_i = \frac{1}{1 + k_{d,i}t} \quad n_i = 2 \quad [8]$$

The rate coefficient $k_{d,i}$ can be related to a decay time $t_{c,i}$ (s) which is the time constant for the activity decay where the order n_i equals 1 and to the half-life time in the case where the order n_i equals 2.

$$t_{c,i} = \frac{1}{k_{d,i}} \quad [9]$$

(b) Model discrimination at 823 K. Expressions [1], [4], [7], and [8] served as a basis for the simulation of the evolution of the adsorption rate coefficient of methane k_a and of the conversion x. The kinetic parameters were estimated for several possible combinations of reaction orders n_i. The parameter optimization was always started using the Rosenbrock search. Closer to the minimum of the objective function the Marquardt method was more efficient. The latter routine also contained a module for the statistical tests of the results.

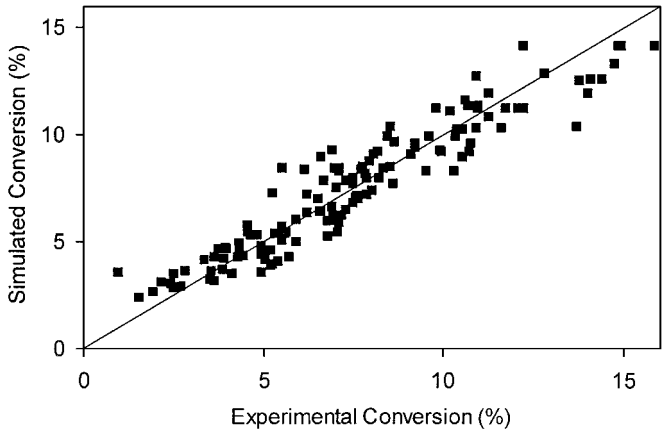

FIG. 8. Parity plot of the experimental and simulated conversion observed during experiments on 0.060 g of surface-oxidized Ni catalyst at 823 K, described in Section 3.4.1.a.

The model discrimination for the adsorption of methane on the sites $l_{100\,s}$ and $l_{1000\,s}$ was based upon regression of all the results obtained with 0.060 g of surface oxidized Ni catalyst at 823 K (Section 3.4.1.a), and that for the adsorption of methane on $l_{10\,s}$ upon regression of experimental data obtained with 0.20 g of surface-oxidized catalyst (Section 3.4.1.b). The best fit was obtained when the rate of decay of the activity for methane adsorption is second order with respect to θ_i for the sites $l_{10\,s}$ and $l_{100\,s}$ and first order for the sites $l_{1000\,s}$. The fit of some experimental data at 823 K is shown in Figs. 5 to 7. The parity plot of all experimental data described in Section 3.4.1.a is shown in Fig. 8. Table 4 is a summary of the kinetic parameters and the 95% confidence intervals for the adsorption of methane on $l_{100\,s}$ and $l_{1000\,s}$. The model discrimination for the adsorption of methane on $l_{10\,s}$ was based upon the experiments performed at different temperatures, described in the following section.

(c) Adsorption kinetics between 723 and 823 K. Analogous experiments as described in Section 3.4 were performed at 723, 748, 773, 798, and 823 K. These experiments were also repeated with a larger amount of catalyst, i.e., 0.20 g of Ni catalyst. This allowed the conversion to be accurately measured at temperatures below 823 K. The model with $n_{10\,s}$ and $n_{100\,s}$ equal to 2 and $n_{1000\,s}$ equal to 1 was fitted

TABLE 4

Parameter Estimates and 95% Confidence Intervals for the Adsorption Model of Methane on $l_{100\,s}$ and $l_{1000\,s}$, Determined by Regression of the Experimental Results Obtained at 823 K on 0.060 g of Ni Catalyst (Section 3.4.1.a)

	$l_{100\,s}$	$l_{1000\,s}$
n_i	2	1
$k_{a,i}$ ($m_r^3\ kg_c^{-1}\ s^{-1}$)	0.0178 ± 0.002	0.0283 ± 0.002
$t_{c,i}$ (s)	329 ± 130	6410 ± 900

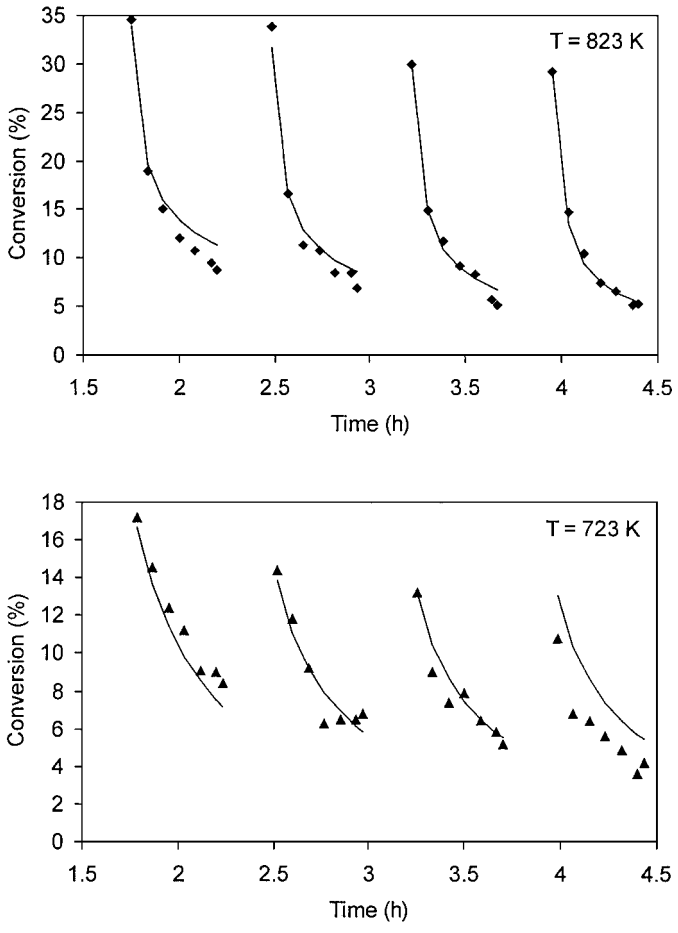

FIG. 9. Experimental and simulated methane conversion at 823 and 723 K on 0.20 g of surface-oxidized catalyst as a function of time following surface oxidation. Oxygen was fed (10^{-6} mol s^{-1}) for 10 min every 45 min. (—) Modeled according to Section 3.4.2.c.

to the experimental results. Figure 7 and Fig. 9 show the fit between the experimental and simulated conversions and adsorption rate coefficients at different temperatures. The parity plot of all experimental data obtained during the experiments at different temperatures is shown in Fig. 10.

Table 5 shows the estimated kinetic parameters for the adsorption of methane on $l_{10\,s}$, $l_{100\,s}$, and $l_{1000\,s}$ in the temperature interval 723 to 823 K. In Section 3.5, it will be argued that the decay of the methane adsorption rate via the sites $l_{10\,s}$ and $l_{100\,s}$ under vacuum is caused by the desorption of oxygen. The rate of desorption is proportional to the square of the concentration of adsorbed oxygen from which it is deduced that the rate-determining step is the recombination of dissociated oxygen. The half-life time at 823 K of oxygen on the surface under vacuum after saturation is respectively 4.8 and 148 s for $l_{10\,s}$ and $l_{100\,s}$. The desorption of oxygen adsorbed on $l_{10\,s}$ is not activated. The activation energy of desorption of oxygen from $l_{100\,s}$ is 96 kJ mol^{-1}. From their broadened-pulse experiments, Hu and Ruckenstein (17) concluded that the adsorption of methane proceeds via reaction with chemisorbed oxygen. They observed that the methane, oxygen, and CO_2 responses coincide with the inert argon response. This can also be explained by a rapid saturation of the NiO surface with oxygen and by rapid surface reactions. The results shown in Section 3.6 indicate that oxygen present in CO_2 originates from the bulk and not directly from oxygen chemisorbed on the surface. The results presented here clearly show a direct correlation between the methane adsorption rate and the amount of adsorbed oxygen.

The concentration of sites $l_{1000\,s}$ decays according to a first-order dependency with respect to the time the catalyst is held under vacuum and is independent of the concentration of gas-phase oxygen. The time constant for the concentration decay is 6250 s at 823 K. Sintering of the NiO on the alumina can explain the slow decay in concentration of the sites $l_{1000\,s}$. This, however, contradicts the observation that after saturation with oxygen the methane adsorption rates on $l_{10\,s}$ and $l_{100\,s}$ are independent of the concentration of sites $l_{1000\,s}$. Also, an analysis of the results of Gavalas *et al.* (15, 16) shows that a decreasing exponential function can describe the evolution of the methane conversion as a

TABLE 5

Parameter Estimates and 95% Confidence Intervals for the Adsorption Model of Methane on $l_{10\,s}$, $l_{100\,s}$, and $l_{1000\,s}$ Determined by Regression of the Experimental Results Obtained between 723 and 823 K on 0.20 g of Ni Catalyst

	$l_{10\,s}$	$l_{100\,s}$	$l_{1000\,s}$
n_i	2	2	1
$k_{a,i}$ (m_r^3 kg_c^{-1} s^{-1}) at 823 K	0.031 ± 0.002	0.027 ± 0.002	0.025 ± 0.008
$E_{ka,i}$ (kJ mol^{-1})	103 ± 13	29.5 ± 6.4	45.0 ± 5.2
$t_{c,i}$ (s) at 823 K	4.78 ± 0.94	148 ± 36	6250 ± 1800
$E_{kd,i}$ (kJ mol^{-1})	0.0 (15 ± 39)	96 ± 19	-62 ± 39

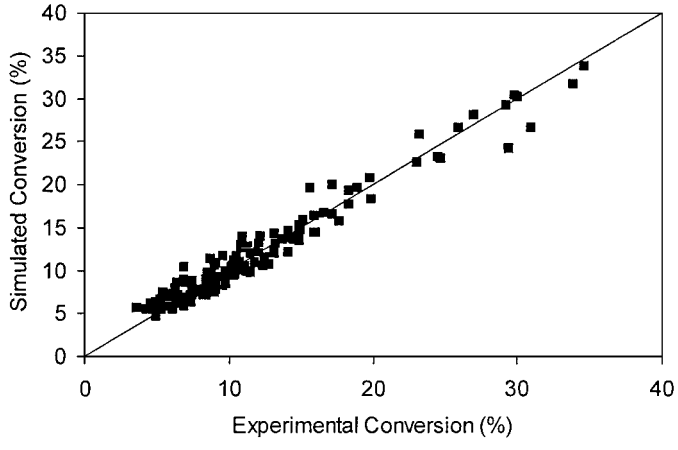

FIG. 10. Parity plot of the experimental and simulated conversion observed in experiments with 0.20 g of surface-oxidized Ni catalyst at 823, 798, 773, 748, and 723 K.

function of time over both a Ni/Al_2O_3 catalyst and a Ni/ZrO_2 catalyst on the time scale of 1000 s. For both supports, a mean lifetime of the activity of about 2 h at 998 K is derived. This shows that the support has no influence on the activity decay and that sintering of the NiO particles is not responsible for the observed activity decay of $l_{1000\,s}$. As has been argued in the literature, the latter is probably caused by the decrease in the amount of excess O^{2-} in the NiO lattice and in the corresponding decrease in concentration of Ni^{3+} (15, 16). The activation energy for the decay of the rate of the methane adsorption on $l_{1000\,s}$ is -62 kJ mol^{-1}. This negative value could result from a high activation energy for the diffusion of O^{2-} to the surface compared to the activation energy for desorption of this oxygen, once it reaches the surface. Consider the continuity equations for the excess oxygen in the bulk and on the surface of the NiO [10].

$$\begin{aligned} D_{\text{bulk}}\frac{\partial^2 C_{\text{bulk}}}{\partial r^2} &= \frac{\partial C_{\text{bulk}}}{\partial t} \quad t>0, 0<r<+\infty \\ C_{\text{bulk}} &= C_{i,\text{bulk}} \quad t=0, 0<r<+\infty \\ \frac{\partial C_{\text{bulk}}}{\partial r} &= 0 \quad t>0, r=+\infty. \\ \frac{\partial C_{\text{surf}}}{\partial t} &= D_{\text{bulk}}\frac{\partial C_{\text{bulk}}}{\partial r} - k_d C_{\text{surf}} \quad t>0, r=0 \\ C_{\text{surf}} &= C_{i,\text{surf}} \quad t=0 \end{aligned} \qquad [10]$$

Equilibrium dissolution of adsorbed oxygen in the bulk of the NiO can be written

$$\frac{C_{\text{i,bulk}}}{C_{\text{i,surf}}} = \frac{C_{\text{bulk}}}{C_{\text{surf}}} = H \quad t\geq 0, r=0. \qquad [11]$$

D_{bulk} ($m_c^2\,s^{-1}$) is the diffusivity of O^{2-} in the NiO lattice, C_{bulk} and $C_{\text{i,bulk}}$ (mol m_c^{-3}) are the bulk concentration and the initial bulk concentration of excess O^{2-}, while C_{surf} and $C_{\text{i,surf}}$ (mol m_c^{-2}) are the concentration and the initial concentration of adsorbed oxygen, and r (m_c) is the depth in the NiO lattice. H (m_c^{-1}) is the Henry coefficient for dissolution of adsorbed oxygen in the NiO bulk.

Assuming that oxygen desorption is much faster than diffusion of oxygen from the bulk to the surface, Laplace transformation of [10] and [11] with respect to time yields

$$\frac{C_{\text{s,surf}}}{C_{\text{i,surf}}} \approx \frac{1}{s+k_{\text{d}}} + \sqrt{\frac{H^2 D_{\text{bulk}}}{s}}\frac{1}{s+k_{\text{d}}}, \qquad [12]$$

in which s is the Laplace ordinate (s^{-1}) and $C_{\text{s,surf}}$ is the Laplace transform of the concentration adsorbed oxygen.

The above equation shows that the decay time t_c is inversely proportional to the square of the desorption rate coefficient k_d, while it is proportional to the bulk diffusion coefficient and to the square of the Henry coefficient for dissolution of adsorbed oxygen in the bulk provided the decrease of C_{surf} is considered on a time scale s^{-1} larger than k_{d}^{-1} [13].

$$t_{\text{c}} \propto \frac{H^2 D_{\text{bulk}}}{k_{\text{d}}^2}. \qquad [13]$$

From this equation, it follows that a negative activation energy for t_c^{-1} is obtained when the activation energy for desorption is lower than half the activation energy for bulk diffusion minus the heat of dissolution of adsorbed oxygen in the NiO bulk.

3.5 Interaction of Oxygen with the Surface-Oxidized Catalyst

In the previous sections, it was shown that several types of active sites for the adsorption of methane exist on NiO/Al_2O_3. It is proposed that the adsorption of methane on two of these sites, $l_{10\,s}$ and $l_{100\,s}$ involves the reaction of methane with chemisorbed oxygen. Most likely, the decay of the methane adsorption rate on these sites with time under vacuum is caused by desorption of oxygen from these sites. The second-order dependency of the rate at which the adsorption rate decreases shows that the desorption of oxygen is recombinative. This would mean that the chemisorbed oxygen is dissociatively adsorbed oxygen. The interaction of oxygen with the surface-oxidized Ni catalyst was therefore studied in more detail.

(a) Interaction of oxygen with the surface-oxidized catalyst on a time scale of 100 s. The interaction of oxygen with the surface-oxidized Ni/Al_2O_3 catalyst on a time scale of 100 s was studied by means of titration experiments. In these experiments, 0.20 g of Ni catalyst, oxidized at 823 K, was saturated with oxygen at 823 K by means of an oxygen pulse train. Each oxygen pulse contained 4×10^{16} molecules. The oxygen uptake of the catalyst is shown as a function of time after saturation in Fig. 11. Based upon Eqs. [5] and [6], the following equation can be derived for the amount of

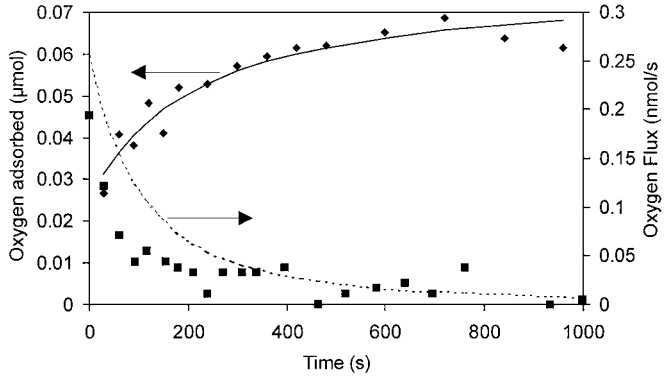

FIG. 11. Evolution of the amount of oxygen adsorbed during pulse titration (◆) and evolution of the oxygen flux (■) as a function of time after saturation. (— and – – –) Simulated according to Section 3.5.a.

TABLE 6

Parameter Estimates and 95% Confidence Intervals for the Desorption of Oxygen on a Time Scale of 100 s at 823 K

$N_{100\,s}$ (10^{-8} mol)	5.28 ± 0.86
$N_{10\,s}$ (10^{-8} mol)	2.46 ± 0.84
$t_{c,100\,s}$ (s)	207 ± 102

oxygen N_{ads} (mol) that can be readsorbed on the catalyst as a function of time under vacuum after saturation with oxygen. The equation is valid only for the results obtained on a time scale of 100 s. $N_{10\,s}$ and $N_{100\,s}$ are the amounts of adsorbed oxygen disappearing on a time scale of respectively 10 and 100 s.

$$N_{ads} = N_{100\,s}\left(1 - \frac{1}{1 + \frac{t}{t_{c,100\,s}}}\right) + N_{10\,s}. \qquad [14]$$

The amount of oxygen adsorbing on $l_{10\,s}$ and $l_{100\,s}$ and the desorption rate constant $k_{d,100\,s}$ or the decay time $t_{c,100\,s}$ can be estimated from the experimental results by means of regression using Eq. [14]. The parameters are shown in Table 6. The decay time $t_{c,100\,s}$ observed here corresponds with the decay time estimated from the methane adsorption experiments. This shows that the decay in the methane adsorption rate is caused by a decrease in the amount of adsorbed oxygen resulting from recombinative desorption of dissociated oxygen: desorption of oxygen was indeed detected on a time scale of 100 s (Fig. 11). The dotted line in Fig. 11 is the simulated flux of oxygen at the exit of the reactor, calculated using the kinetics estimated from the saturation experiments described above. The correspondence is reasonable. These results confirm that the adsorption of methane on the sites $l_{100\,s}$ proceeds via interaction of gas-phase methane with oxygen reversibly and dissociatively chemisorbed on the active sites. The decay of the methane adsorption rate on these sites under vacuum is caused by desorption of the adsorbed oxygen. The concentration $C_{t,100\,s}$ (mol kg_c^{-1}) of active sites $l_{100\,s}$ is 5.03×10^{-4} mol kg_c^{-1}, i.e., about 2% of the amount of available Ni sites on the surface (Table 6).

(b) Interaction of oxygen with the surface-oxidized catalyst on a time scale of 10 s. Single pulse experiments on a time scale of 10 s were performed to check if there is also oxygen reversibly chemisorbed on the catalyst and desorbing on a time scale of 10 s. Oxygen pulses were injected over 0.21 g of surface-oxidized Ni/Al_2O_3 at 823 K. The Ni catalyst was oxidized at 823 K. The oxygen pulse contained 1.0×10^{15} or 2.6×10^{15} molecules of oxygen. Oxygen was found to strongly adsorb on the catalyst (Fig. 12). The pulse frequency was too low to accurately measure the responses. The results, however, show that oxygen desorbs from the catalyst on a time scale similar to the scale at which the activity of the sites $l_{10\,s}$ decays under vacuum after saturation of the catalyst with oxygen. The amount of active sites can be calculated from the parameters presented in Table 6. The concentration of active sites $l_{10\,s}$ is estimated from $N_{10\,s}$ to be about 2.34×10^{-4} mol kg_c^{-1}, i.e., about 1% of the amount of available Ni sites on the surface. The concentration of sites $l_{100\,s}$ and $l_{10\,s}$ do not differ more than a factor of 2, so that they can be considered as two different sites. Indeed, if two oxygen species would exist on the same type of site, a much larger difference in concentration would be expected, considering the large difference in lifetime on the surface.

3.6. Reaction of Methane and Oxygen on the Surface-Oxidized Catalyst

The oxidation of methane on the Ni catalyst surface oxidized at 823 K was studied by means of experiments which mainly consisted of step experiments with CH_4 and isotopically labeled oxygen. Only water and CO_2 were detected as products. Step experiments with CH_4 over the Ni catalyst oxidized with $^{16}O_2$ show that both $l_{10\,s}$ and $l_{100\,s}$ activate the transformation of methane to water and CO_2. The step responses depend on the time elapsed between feeding oxygen over the oxidized catalyst and feeding methane. The results of Gavalas *et al.* (15, 16) show that the activation of methane on $l_{1000\,s}$ leads to the production of CO_2 and H_2O. The amount of water produced is very low during the methane step in the absence of gas-phase oxygen. When a CH_4 step is fed over the oxidized catalyst in the presence of gas-phase oxygen, a much higher methane conversion and an important water response is observed (Fig. 13). The strong increase of the water response in the presence of oxygen seems to be caused by the higher

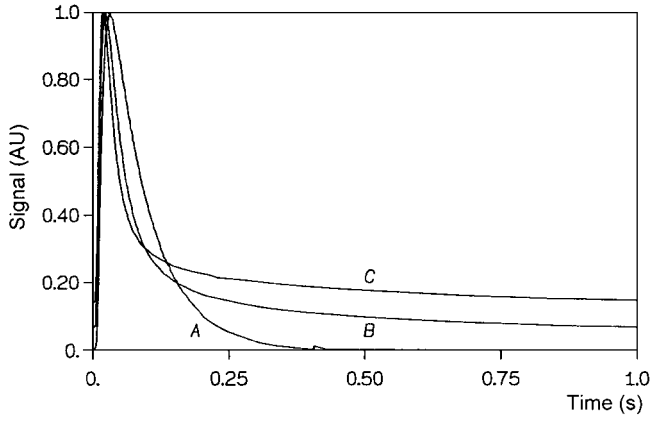

FIG. 12. Normalized periodic oxygen and argon pulse responses on O_2/Ar pulses at 823 K on 0.21 g of surface-oxidized Ni catalyst. (A) Agon; (B) O_2, 2.6×10^{15} molecules; (C) O_2, 1.0×10^{15} molecules.

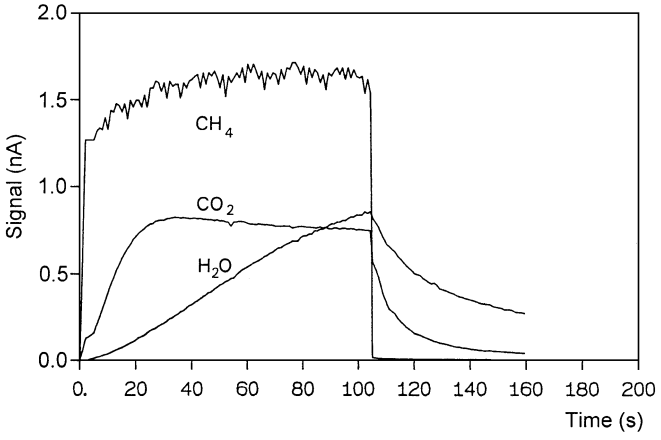

FIG. 13. Responses of a methane step (1.1×10^{-8} mol s^{-1}) in an oxygen flow (10^{-7} mol s^{-1}) at 823 K on 0.21 g of surface-oxidized Ni catalyst.

methane conversion. This is an indication that recombination of hydroxyl groups on the NiO surface is a kinetically significant step in the production of water. Further insight in the mechanism of the combustion of methane on NiO/Al_2O_3 was obtained from step experiments of $CH_4/^{16}O_2$ over the Ni catalyst surface oxidized at 823 K with $^{18}O_2$. The results are shown in Fig. 14. The $C^{18}O_2$ response rapidly breaks through. It is followed by a slow decay which correlates with the decrease of ^{18}O in the oxygen flow at the exit of the reactor. The $C^{16}O_2$ breakthrough requires much more time and the increase is much slower. This shows that the lattice oxygen is involved in the C–O bond formation. The water responses have the same shape, independent of the isotopic composition. Chemisorbed oxygen would be active in the abstraction of hydrogen from methane and adsorbed CH_x species, resulting in the formation of water through the condensation of the produced hydroxyl groups. This means that water is a primary product on NiO. A mechanism for the combustion of methane on the oxidized Ni catalyst in agreement with the results presented above is shown in Fig. 15. O_S represents oxygen adsorbed on $l_{10\,s}$ or $l_{100\,s}$ or excess lattice oxygen at the surface, corresponding to $l_{1000\,s}$. O_L is lattice oxygen. The subscript s is used to denote intermediates on the surface. Combining this mechanism with the reforming mechanism on a reduced Ni catalyst proposed by Xu and Froment (10) results in a complete mechanism for the catalytic partial oxidation of methane to synthesis gas on Ni catalysts.

4. CONCLUSION

The activation of methane on an industrial Ni/Al_2O_3 catalyst was studied in a TAP reactor. The reduced catalyst shows a high activity for methane adsorption. The activation energy for methane adsorption is estimated to be 54 kJ mol^{-1}. The surface-oxidized catalyst is 10 to 20 times less active for methane adsorption than the reduced catalyst. The activity of the reduced catalyst rapidly decays as a function of the degree of oxidation. Three different sites for methane adsorption were observed after surface oxidation of the catalyst at 823 K. Methane adsorption on two of the three active sites should proceed via hydrogen abstraction from gas phase methane by adsorbed oxygen. The adsorbed oxygen has a half-life time of 5 and 148 s at 823 K. The third type of active site disappears or deactivates according to first-order kinetics and has a mean lifetime of 6300 s at 823 K. These sites are probably created by over-oxidation of the reduced Ni catalyst, resulting in the formation of Ni^{3+} cations. A mechanism for the combustion of methane is proposed. Chemisorbed oxygen is involved in the H abstraction from methane or from adsorbed intermediates. Lattice oxygen is responsible for the formation of the carbon-oxygen bond in CO_2. The structure of the Ni catalyst was continuously monitored by means of

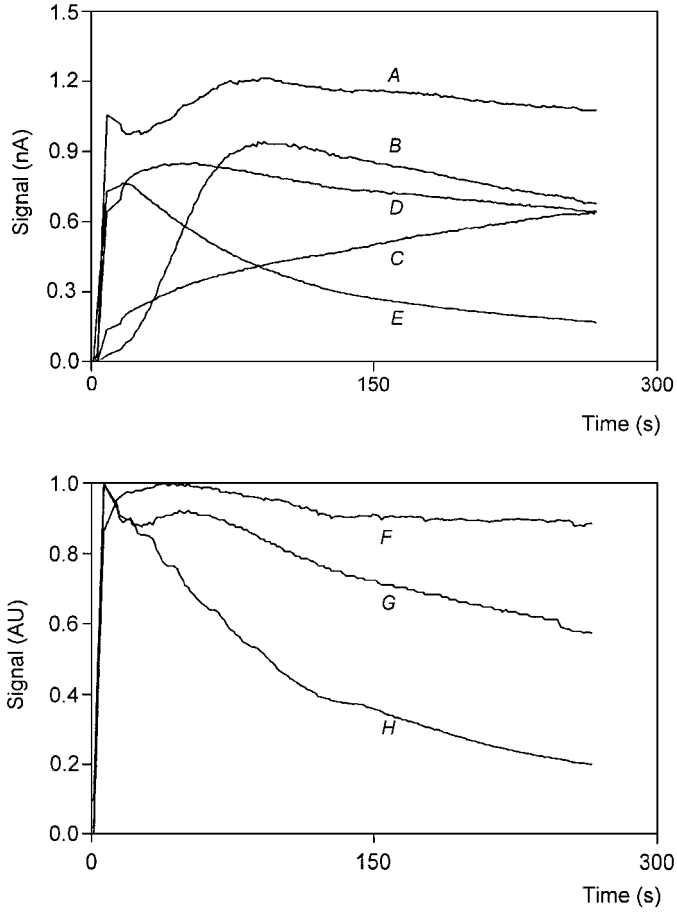

FIG. 14. Responses to a $CH_4/^{16}O_2$ step at 823 K immediately following the disconnection of the $^{18}O_2$ feed over a $Ni^{18}O/Al_2O_3$ sample stabilized during 3 h after surface oxidation. (A) 0.5 $H_2{}^{16}O$ + important contribution $^{18}O_2$; (B) $H_2{}^{18}O$; (C) $C{}^{16}O_2$; (D) $C{}^{16}O{}^{18}O$; (E) $C{}^{18}O_2$; (F) $^{16}O_2$; (G) $^{16}O{}^{18}O$; (H) $^{18}O_2$.

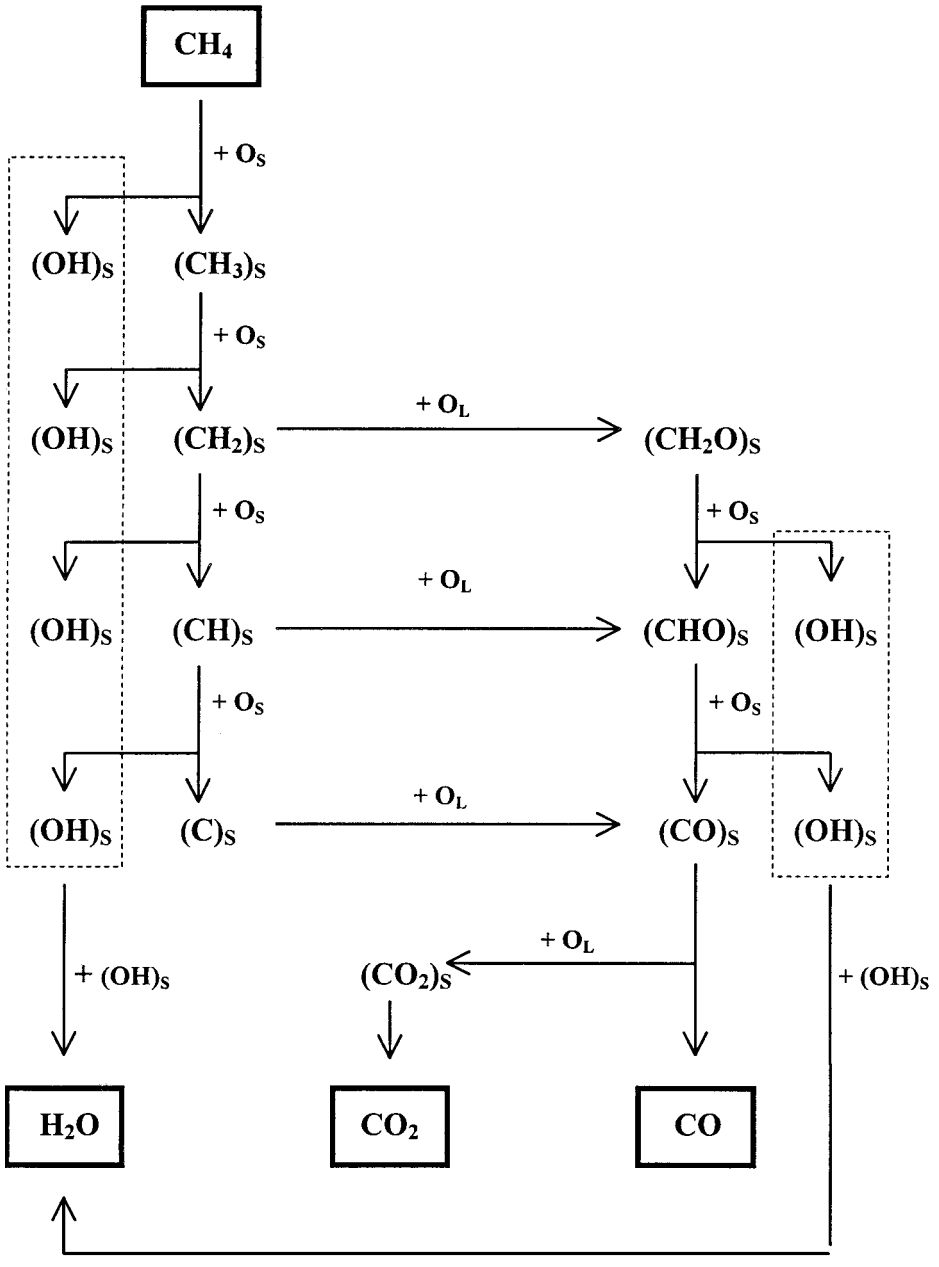

FIG. 15. Reaction scheme for the combustion of methane on NiO/Al_2O_3.

TPR. After TPR up to 1138 K, the Ni catalyst exhibits large and small Ni crystallites on the Al_2O_3 support but also Ni crystallites in the Al_2O_3 support. The small Ni crystallites are not active toward methane after reduction at high temperatures. This suggests that they are partially covered by a thin layer of Al_xO_y which does not exclude oxygen adsorption on these crystallites. Oxidation at 823 K results in a NiO catalyst in which the large Ni crystallites are reoxidized to NiO and the small crystallites to $NiAl_2O_4$ surface spinel. The spinel was found to be inactive toward methane.

APPENDIX: NOMENCLATURE

Roman Symbols

C_{bulk}	bulk concentration of excess O^{2-} (mol m_c^{-3})
$C_{i,bulk}$	initial bulk concentration of excess O^{2-} (mol m_c^{-3})
C_{CH_4}	gas-phase concentration methane (mol m_g^{-3})
C_{surf}	concentration of adsorbed oxygen (mol m_c^{-2})
$C_{i,surf}$, $C_{t,surf}$	initial and maximum concentration of adsorbed oxygen (mol m_c^{-2})

$C_{t,i}$ concentration sites l_i (mol kg_c^{-1})
D_{bulk} diffusivity of O^{2-} in the NiO lattice ($m_c^2\ s^{-1}$)
D_c, D_e Knudsen diffusion coefficient in the catalyst and exit packing ($m_g^3\ m_r^{-1}\ s^{-1}$)
i index 10 s, 100 s, or 1000 s
H Henry coefficient for dissolution of adsorbed oxygen in the bulk NiO (m_c^{-1})
k_a adsorption rate coefficient of methane ($m_r^3\ kg_c^{-1}\ s^{-1}$)
$k_{a,i}$ adsorption rate coefficient on site l_i at full coverage or presence ($m_r^3\ kg_c^{-1}\ s^{-1}$)
k_d desorption rate coefficient (s^{-1})
$k_{d,i}$ desorption or deactivation rate coefficient from site l_i (s^{-1})
L_c, L_e length of the catalyst bed and the exit packed section (m_r)
n_i order of $r_{d,i}$ with respect to θ_i
N_{ads} total amount of O_2 desorbed (mol)
Ni_s surface Ni atoms
$N_{10\,s}$ amount of O_2 desorbing on a time scale of 10 s (mol)
$N_{100\,s}$ amount of O_2 desorbing on a time scale of 100 s (mol)
r depth in the NiO lattice (m_c)
r_a adsorption rate of methane (mol $kg_c^{-1}s^{-1}$)
$r_{a,i}$ adsorption rate of methane on site l_i (mol $kg_c^{-1}\ s^{-1}$)
$r_{d,i}$ desorption rate of oxygen from $l_{10\,s}$ and $l_{100\,s}$ or the disappearance rate of $l_{1000\,s}$ (mol $kg_c^{-1}\ s^{-1}$)
s Laplace ordinate (s^{-1})
t time (s)
$t_{c,i}$ characteristic decay time of oxygen chemisorbed on site l_i or characteristic decay time of the activity of the sites l_i (s)
x conversion

Greek Symbols

ε_c void fraction of the catalyst and exit packed section ($m_g^3\ m_r^{-3}$)
θ_i coverage of site $l_{10\,s}$ or $l_{100\,s}$ with oxygen or fraction of the sites $l_{1000\,s}$ still active
ρ_B bulk density of the catalyst bed ($kg_c\ m_r^{-3}$)

ACKNOWLEDGMENTS

Olivier Dewaele acknowledges the Fund for Scientific Research—Flanders for a research assistant fellowship. Prof. Lucien Fiermans is gratefully acknowledged for the XRD and XPS experiments performed at the Department of Solid State Sciences of the University of Ghent. Sophie Van Dyck is acknowledged for help during the experiments.

REFERENCES

1. Bharadwaj, S. S., and Schmidt, L. D., *J. Catal.* **146**, 11 (1994).
2. Dissanayake, D., Ronyek, M. P., Kharas, K. C. C., and Lunsford, J. H., *J. Catal.* **132**, 117 (1991).
3. Chu, Y., Li, S., Lin, J., Gu, J., and Yang, Y., *Appl. Catal. A* **134**, 67 (1996).
4. van Looij, F., and Geus, J. W., *J. Catal.* **168**, 154 (1997).
5. Beebe, T. P., Goodman, D. W., and Kay, B. D., *J. Chem. Phys.* **87**, 2305 (1987).
6. Alstrup, I., Chorkendorff, I., and Ullmann, S., *Surf. Sci.* **234**, 79 (1990).
7. Lee, M. B., Yang, Q. Y., Tang, S. L., and Ceyer, S. T., *J. Chem. Phys.* **85**, 1693 (1986).
8. Schouten, F. C., Kaleveld, E. W., and Bootsma, G. A., *Surf. Sci.* **63**, 400 (1977).
9. Krishnan, G., and Wise, H., *Appl. Surf. Sci.* **37**, 224 (1989).
10. Xu, J., and Froment, G. F., *AIChE J.* **35**, 88 (1989).
11. Beckerle, J. D., Yang, Q. Y., Johnson, A. D., and Ceyer, S. T., *J. Chem. Phys.* **86**, 7236 (1987).
12. Holloway, P. H., and Hudson, J. B., *Surf. Sci.* **43**, 43 (1974).
13. Holloway, P. H., and Hudson, J. B., *Surf. Sci.* **43**, 141 (1974).
14. Horgan, A. M., and Kung, D. A., *Surf. Sci.* **23**, 259 (1970).
15. Gavalas, G. R., Phichitkul, C., and Voecks, G. E., *J. Catal.* **88**, 54 (1984).
16. Gavalas, G. R., Phichitkul, C., and Voecks, G. E., *J. Catal.* **88**, 65 (1984).
17. Hu, Y. H., and Ruckenstein, E., *J. Phys. Chem. B* **102**, 230 (1998).
18. Gleaves, J. T., Ebner, J. R., and Kuechler, T. C., *Catal. Rev. Sci. Eng.* **30**, 1 (1988).
19. Müller, J., *J. Catal.* **6**, 50 (1966).
20. Hoang-Van, C., Kachaya, Y., Teichner, S. J., Arnaud, Y., and Dalmon, J. A., *Appl. Catal.* **46**, 281 (1989).
21. Zielinski, J., *J. Catal.* **76**, 157 (1982).
22. Huang, Y. J., Schwarz, J. A., Diehl, J. R., and Baltrus, J. P., *Appl. Catal.* **37**, 229 (1988).
23. De Bokx, P. K., Wassenberg, W. B. A., and Geus, J. W., *J. Catal.* **104**, 86 (1987).
24. Rynkowski, J. M., Paryjczak, T., and Lenik, M., *Appl. Catal. A* **106**, 73 (1992).
25. De Deken, J., Ph.D. thesis, University of Ghent, 1982.
26. De Bokx, P. K., Kock, A. J. H. M., Boellaard, E., Klop, W., and Geus, J. W., *J. Catal.* **96**, 454 (1985).
27. Wang, D., Dewaele, O., and Froment, G. F., *J. Mol. Catal.* **136**, 299 (1998).
28. Schouten, F. C., Gijzeman, O. L. J., and Bootsma, G. A., *Surf. Sci.* **87**, 1 (1979).
29. De Groote, A. M., and Froment, G. F., *Appl. Catal. A* **138**, 245 (1996).
30. Hutchings, G. J., and Scurrell, M. S., *in* "Methane Conversion by Oxidative Processes, Fundamental and Engineering Aspects" (E. E. Wolf, Eds.). Van Nostrand Reinhold, New York, 1992.
31. Kung, H. H., *in* "Studies in Surface Science and Catalysis" (B. Delmon and J. T. Yates, Eds.), Vol. 45, p. 1. Elsevier, Amsterdam, 1989.
32. Boreskov, G. K., *in* "Catalysis. Science and Technology" (J. R. Anderson and M. Boudart, Eds.), Vol. 3, p. 39. Springer, Berlin, 1982.
33. Bielanski, A., and Najbar, M., *J. Catal.* **25**, 398 (1972).